Exact eddy-viscosity equation for turbulent wall flows

Emmanuel Plaut[1] **& Stefan Heinz**[2]
[1]Université de Lorraine, CNRS, LEMTA, F-54000 Nancy, France
[2]Mathematics Department, University of Wyoming, Laramie, WY, USA

Confidential draft **PlautHeinz20.pdf** - Version 0.11 of June 18, 2020

Table of contents

What's new in this Version 0.11 of June 18, 2020

- I created the section 4.3.

Abstract

A recent theory has been developed (Heinz 2018, 2019) for three canonical turbulent wall flows: channel flow, pipe flow and zero-pressure gradient boundary layer, that offers exact analytical formulas for the RANS eddy-viscosity, as a product of a function of y^+ (the wall-normal distance scaled in inner units) with functions of y/δ (the same distance scaled in outer units). By calculating the eddy-viscosity turbulent diffusion term for these flows where the turbulence is stationary, one identifies a high-Reynolds number RANS eddy-viscosity equation with one production and two dissipation terms. One dissipation term is universal, peaks in the near-wall region, and scales mainly with y^+. The second one, smaller in magnitude, is flow-dependent, peaks in the wake region, and scales mainly with y/δ. The production term is flow-dependent, peaks in between, and scales also mainly with y/δ. The universal dissipation term implies a damping function and a length scale analogous to the von Karman length scale used in the Scale-Adaptative Simulation models. This length scale also appears in the production term. This confirms on firm theoretical bases the relevance of von Karman length scales. This is an occasion to analyze these length scales in more details. An asymptotic analysis of all terms in the eddy-viscosity budget in the limit of infinite Reynolds numbers is also proposed. This allows a review and tests of existing RANS models that imply an eddy-viscosity equation. Finally, we propose a new version of the eddy-viscosity equation of the Scale-Adaptative Simulation models.

---

1 Introduction (with a list of physical questions)

To be written !.. In this draft, I list some physical questions that we want to address, and how we answer them.

1. For turbulent wall flows, does production in the ν_t equation mainly scale with y/δ ?

   → yes, see the sections 3.2, 3.3, 3.4 and 3.6.

2. For turbulent wall flows, does dissipation in the ν_t equation mainly scale with y^+ ?

   → yes, for the near-wall contribution which corresponds to its peak, see the sections 3.2, 3.3, 3.4 and 3.5.

3. For turbulent wall flows, what happens as $Re_\tau \to \infty$?

   → all terms in the ν_t equation (budget) have well-identified limits, that are either functions of y^+ or y/δ, see the sections 3.5, 3.6 and 3.7.

4. How does the production term in the ν_t equation differ for the three turbulent wall flows ?

   → answer at the end of the section 3.6.

5. By studying existing models with a ν_t equation, can one show that some of these models require length-scale information ?

   → regarding the models of Spalart & Allmaras (1994); Yoshizawa *et al.* (2012): yes, see the section 4.

6. Inspired by all this, can one propose a new general eddy-viscosity equation for wall-bounded turbulent flows, that would yield for channel flows at least better results than existing models ?

   → *unclear, first steps are studied in the section 4 !..*

2 Flow cases and state of the art

2.1 Turbulent wall flows

A part of the text below, especially of the first sentences, will probably move to the introduction...

Wall-bounded turbulent flows are ubiquitous in human-made fluid systems, and are also encountered in the nature: the atmospheric boundary layer for instance is the place where we live and where we like to set up buildings, wind turbines, etc. In the infinite family of these flows, one may distinguish three canonical cases: channel flow, pipe flow and the zero-pressure gradient turbulent boundary layer, or 'boundary layer', for the sake of concision. These flows, denoted here 'turbulent wall flows', are somewhat simpler, because the geometry of the fluid domain is simple and highly symmetric, but they still present a good richness of behaviour. We will build an exact eddy-viscosity equation for these three cases, and discuss the possible consequences on other classical models. Before presenting those, let us

fix the hypotheses and notations. We consider an incompressible fluid of mass density ρ and kinematic viscosity ν. In wall-bounded turbulent flows in general, locally a cartesian system of coordinates $Oxyz$ is used, such that x points in the streamwise direction, and y measures the distance to the closest wall. To lowest order, the mean flow

$$\mathbf{U} \;=\; U(y,t)\;\mathbf{e}_x \tag{1}$$

where $\mathbf{e}_x$ is the unit vector in the x-direction, t time. A relevant quantity is the mean strain rate

$$S \;=\; \partial U/\partial y\;, \tag{2}$$

which may be evaluated in more general three-dimensional flows from the full strain-rate tensor, see e.g. the equation (20) of Menter (1997). Focusing now onto the canonical turbulent wall flows, the length scale δ is the half-channel height, pipe radius, or 99% boundary layer thickness with respect to channel flow, pipe flow, and boundary layer, respectively. Denoting $u_x\mathbf{e}_x + u_y\mathbf{e}_y + u_z\mathbf{e}_z$ the fluctuating velocity, the RANS eddy viscosity

$$\nu_t = -\left\langle u_x u_y\right\rangle / S \tag{3}$$

where the angular brackets denote the Reynolds average. The mean wall shear stress τ_w is used to define the friction velocity $u_\tau = \sqrt{\tau_w/\rho}$. From this are defined wall or inner units, i.e. $y^+ = u_\tau y/\nu$, $U^+ = U/u_\tau$ and

$$S^+ \;=\; \partial U^+/\partial y^+\;. \tag{4}$$

Finally, the friction-velocity Reynolds number $Re_\tau \;=\; \delta^+ \;=\; u_\tau\delta/\nu$.

2.2 RANS models with an eddy-viscosity equation

To be written, by citing at least Nee & Kovasznay (1969); Baldwin & Barth (1990); Spalart & Allmaras (1994); Menter (1997); Yoshizawa *et al.* (2012) *...*

2.3 The Scale - Adaptive Simulation models

To be written, by citing at least Menter & Egorov (2006, 2010); Egorov *et al.* (2010); Abdol-Hamid (2015) *!..*
Following Menter & Egorov (2010), *introduce in particular* their turbulent length-scale

$$\ell_t \;=\; c_\mu^{-1/4}\;k^{-1/2}\;\nu_t\;, \tag{5}$$

the von Karman length-scale

$$\ell_{vK} \;=\; \kappa\left|\frac{S}{\partial S/\partial y}\right|\;, \tag{6}$$

with κ the von Karman constant, and their eddy-viscosity equation

$$\frac{\partial\nu_t}{\partial t} \;=\; \frac{1}{\sigma_M}\frac{\partial}{\partial y}\left(\nu_t\frac{\partial\nu_t}{\partial y}\right) \;+\; P_{\nu M} \;-\; D_{\nu M} \tag{7}$$

with

$$P_{\nu M} \;=\; \zeta_1\;\frac{\nu_t^2 S^2}{k}\;, \tag{8a}$$

$$D_{\nu M} \;=\; \zeta_2\;\frac{\nu_t^2 S^2}{k}\left(\frac{\ell_t}{\ell_{vK}}\right)^2 \;+\; c_\mu^{1/4}\zeta_3\;k\;, \tag{8b}$$

$$(\sigma_M,\;\zeta_1,\;\zeta_2,\;\zeta_3) \;=\; (2/3,\;0.8,\;1.47,\;0.0288)\;. \tag{8c}$$

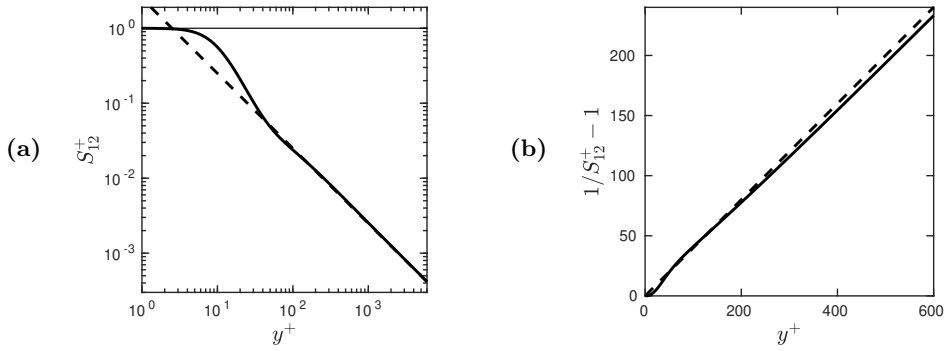

Fig. 1 : **(a)** Continuous line: S_{12}^+ , dashed line: $1/(\kappa y^+)$. **(b)** Continuous line: $1/S_{12}^+ - 1$, dashed line: κy^+.

2.4 Analytic eddy viscosity model of turbulent wall flows

Heinz (2018, 2019) proposed analytic models for the mean flow U, main Reynolds stress $-\langle u_x u_y \rangle$ and eddy viscosity ν_t of the turbulent wall flows defined in section 2.1. In the equation (11) of Heinz (2019), an analytic expression is proposed for the reduced eddy viscosity, which is valid at high Reynolds number, $Re_\tau \gtrsim 500$,

$$\nu^+ \;=\; \nu_t/\nu \;=\; (1/S_{12}^+ - 1)\; W \;. \tag{9}$$

There $S_{12}^+ = S_1^+ + S_2^+$ is a very good approximation of the dimensionless mean strain rate S^+ (4) in the inner region of the flows, i.e., disregarding wake effects, see the equation (7) of Heinz (2018) and the corresponding discussion. Precisely, the universal function

$$S_{12}^+ \;=\; S_{12}^+(y^+) \;=\; 1 \;-\; \left[\frac{(y^+/a)^{b/c}}{1+(y^+/a)^{b/c}}\right]^c \;+\; \frac{1}{\kappa y^+}\,\frac{1+h_2/(1+y^+/h_1)}{1+y_k/(y^+H)} \;, \tag{10}$$

with

$$a = 9, \quad b = 3.04, \quad c = 1.4, \quad H \;=\; H(y^+) \;=\; (1+h_1/y^+)^{-h_2} \;, \quad h_1 = 12.36,\; h_2 = 6.47,\; y_k = 75.8 \;, \tag{11}$$

and the von Karman constant

$$\kappa \;=\; 0.40 \;. \tag{12}$$

The function S_{12}^+ , plotted on the figure 1a, approaches naturally 1 as $y^+ \to 0$ in the viscous sublayer. On the contrary, as $y^+ \to \infty$, $S_{12}^+ \sim 1/(\kappa y^+)$, in agreement with the log law. Therefore the function $1/S_{12}^+ - 1$, plotted on the figure 1b, which appears in the eddy viscosity (9), vanishes in the limit $y^+ \to 0$, and then increases smoothly to approach the function κy^+ as $y^+ \to \infty$.

The second ingredient of the theory is the function W, which is flow-dependent and in outer scaling, because it describes wake effects. With the notations of Heinz (2018, 2019), $W = 1/G_{CP}$ for channel and pipe flows, M_{BL}/G_{BL} for boundary layers, where G_{CP} and G_{BL} characterize the wake contribution S_3^+ to the dimensionless mean strain rate S^+ (see the equations 7 and A.22 of Heinz 2018), M_{BL} characterizes the total stress in boundary layers (see the equation 4 of Heinz 2019). For channel and pipe flows

$$W \;=\; W_X(y/\delta) \quad \text{with} \quad W_X(y) \;=\; \frac{K_X y + (1-y)^2(0.6y^2+1.1y+1)}{1+y+y^2(1.6+1.8y)} \;, \tag{13}$$

$X = C,\; K_C = 0.933$ for channel, $X = P,\; K_P = 0.687$ for pipe; for boundary layers

$$W \;=\; W_{BL}(y/\delta) \quad \text{with} \quad W_{BL}(y) \;=\; \frac{1+0.285\; y\; e^{y(0.9+y+1.09y^2)}}{1+(0.9+2y+3.27y^2)y}\;\; e^{-y^6-1.57y^2} \;. \tag{14}$$

The wake function W is plotted for these three flows on the figure 2a. In the near-wall region, when $y/\delta \to 0$, $W \to 1$, hence the eddy viscosity (9), $\nu^+ \;=\; (1/S_{12}^+(y^+) - 1)\; W(y^+/\delta^+) \;\sim\; (1/S_{12}^+(y^+) - 1)$ where $\delta^+ = Re_\tau$. Therefore the log-layer eddy viscosity κy^+ is approximately recovered if $1 \ll y^+ \ll \delta^+$; for a more precise study, see the section 4.1 of Heinz (2019). When y becomes of the order of δ, wake effects come in, that saturate the growth of the eddy viscosity (9), since W decreases. Whereas the maximum value of y is δ in channel and pipe flows (in channel flow if $y \in [\delta, 2\delta]$ the mean fields can be obtained by suitable symmetries from the mean fields for $y \in [0, \delta]$), it may be much larger in boundary layers. Naturally, $W_{BL} \to 0$ as $y \to \infty$; precisely $W_{BL} < 10^{-3}$ as soon as $y > 1.36\delta$.

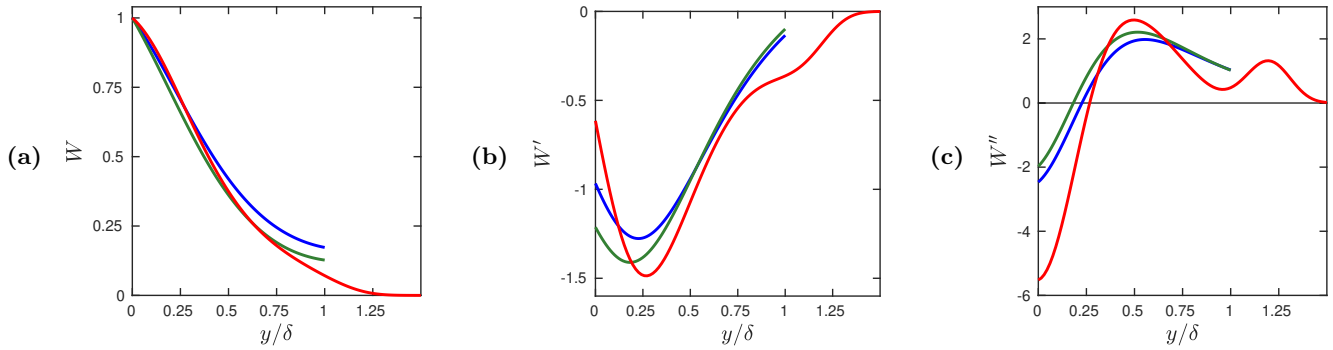

Fig. 2 : **(a)** W **(b)** W' **(c)** W'' for channel (blue), pipe (green), boundary layer (red).

The theory of Heinz (2018, 2019) has been validated by a thorough study of direct numerical simulations (DNS) data, including those of Lee & Moser (2015); Chin *et al.* (2014); Sillero *et al.* (2013), and experimental data, for instance those of Vallikivi *et al.* (2015). For instance, the figures S.6abc of the supplementary material to Heinz (2019) show the eddy viscosity of various DNS, one for each canonical flow, compared with two variants of the eddy-viscosity model (9). In particular, the magenta curves show $\kappa y^+ W$ with our notations, i.e. $(1/S_{12}^+ - 1)$ in (9) has been replaced by κy^+. The agreement with the DNS is good, except in the outer region, where in (3) both the numerator $\langle u_x u_y \rangle$ and the denominator dU/dy tend to zero, hence the DNS noise is amplified.
Since the derivatives W' and W'' will be needed hereafer, they are plotted on the figures 2bc. Whereas the functions W for the three flow cases are quite similar (figure 2a), their first and second derivatives show larger differences (figures 2bc). Naturally, W'_{BL} and $W''_{BL} \to 0$ as $y \to \infty$.

3 Analysis: exact eddy-viscosity equation

3.1 General equation for turbulent wall flows

Since the focus of our study is on high-Reynolds numbers wall-bounded flows, we assume that the form of the eddy-viscosity equation is

$$\sigma \frac{\partial \nu_t}{\partial t} \;=\; \frac{\partial}{\partial y}\Big(\nu_t \frac{\partial \nu_t}{\partial y}\Big) \;+\; P_\nu \;-\; D_\nu \tag{15}$$

with y the wall distance, $P_\nu > 0$ the production, $D_\nu > 0$ the dissipation term. The dimensionless coefficient σ, of order 1, which is a kind of Prandtl number, plays no role in the canonical turbulent wall flows, where the mean fields are steady, but is kept in (15) for the sake of comparison with other turbulence models. In turbulent wall flows, according to (15), the opposite of the turbulent diffusion term

$$-\,T_\nu \;=\; -\,\frac{\partial}{\partial y}\Big(\nu_t \frac{\partial \nu_t}{\partial y}\Big) \;=\; P_\nu \;-\; D_\nu \;. \tag{16}$$

A formal computation of T_ν starting from (9) leads to $D_\nu \;=\; D_{\nu i} \;+\; D_{\nu o}$ and

$$D_{\nu i} \;=\; \kappa^2 \,\frac{\nu_t^2}{L_{vK}^2}\,\frac{1}{f^2}\;, \tag{17a}$$

$$P_\nu \;=\; \kappa\,\frac{\nu_t^2}{L_{vK}\;\delta}\,\frac{1}{1-S_{12}^+}\,\Big(-\,\frac{4W'}{W}\Big) \;=\; \kappa\,\frac{\nu\;\nu_t}{L_{vK}\;\delta}\,\frac{1}{S_{12}^+}\,(-4W')\;, \tag{17b}$$

$$D_{\nu o} \;=\; \frac{\nu_t^2}{\delta^2}\,\frac{W'^2 + WW''}{W^2} \;=\; \frac{\nu^2}{\delta^2}\,(1/S_{12}^+ - 1)^2\,(W'^2 + WW'')\;. \tag{17c}$$

The indices i and o refer to 'inner' and 'outer' terms, respectively, and the notation $D_{\nu o}$ is slightly improper since this term is slightly negative in the near-wall region. However, $D_{\nu o}$ is much smaller in this region than in the outer region where it peaks, as it will be shown in the figure 6b for channel flow, 7b for pipe flow, 8b for boundary layers. Moreover $D_\nu \;=\; D_{\nu i} \;+\; D_{\nu o} > 0$ everywhere, as it will be shown in the figures 6cd for channel flow, 7cd for pipe flow, 8cd for boundary layers, hence the notation D_ν is fully justified.

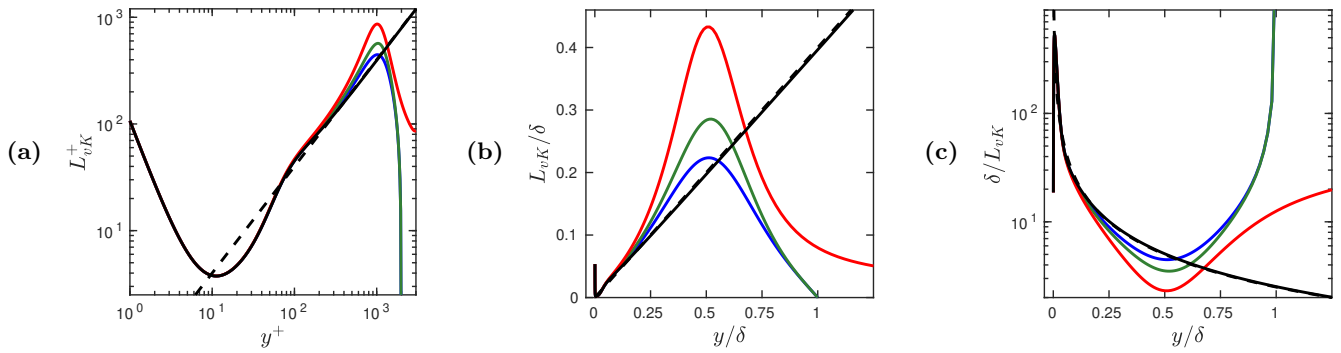

Fig. 3 : **(a,b)** The asymptotic von Karman length scale L_{vK} (18) (black continuous); its log law approximation κy (black dashed); the von Karman length scale ℓ_{vK} (6) for channel (blue), pipe (green), boundary layer (red). The ℓ_{vK}^+ curves of the figure **(a)** and all curves of the figure **(b)** have been computed at $Re_\tau = 1995$. All curves have been computed starting at $y^+ = 1$. The figure **(c)** shows the same curves as figure **(b)** but with the inverse ordinates and linear-log scales.

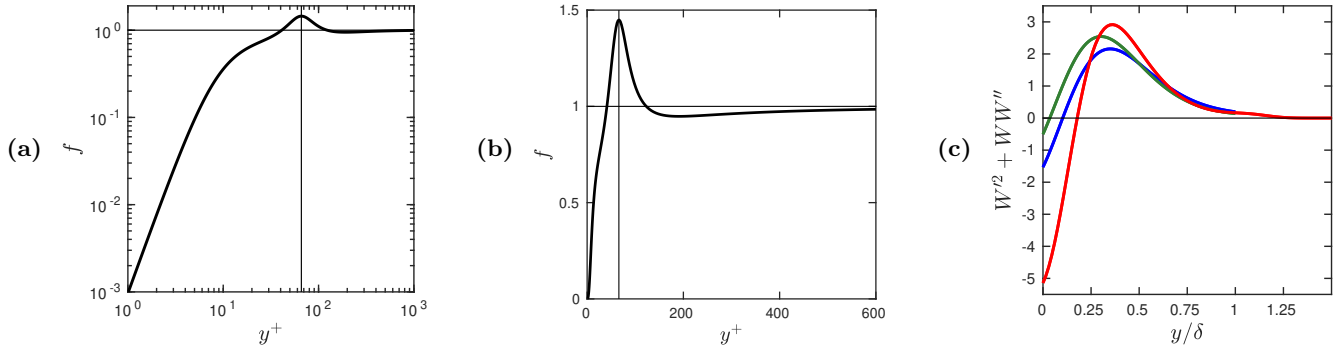

Fig. 4 : **(a,b)** The damping function f. The vertical lines are at $y^+ = 66$. **(c)** The function $W'^2 + WW''$ for channel (blue), pipe (green), boundary layer (red).

In addition to the functions S_{12}^+ and W defined in the section 2.4, there appears in the equations (17) other functions that are built on these. The first one is the asymptotic von Karman length scale

$$L_{vK} \;=\; \kappa \left| \frac{S_{12}}{\partial S_{12}/\partial y} \right| \quad \text{or} \quad L_{vK}^+ \;=\; \kappa \left| \frac{S_{12}^+}{\partial S_{12}^+/\partial y^+} \right| , \tag{18}$$

which is defined as the von Karman length scale ℓ_{vK} (6), but replacing S by S_{12} , i.e., disregarding 'wake effects'. The fact that the length scale L_{vK} appears in (17a) and (17b) confirms on very firm bases the relevance of this length scale, which was not so clear in the works of Rotta. Only the inner-units $L_{vK}^+(y^+)$ is universal, whereas the physical $L_{vK}(y/\delta)$ has to be calculated as $\delta(L_{vK}^+/\delta^+)$, i.e. L_{vK}/δ depends on $\delta^+ = Re_\tau$. Since, as $y^+ \to \infty$, in agreement with the log law, $S_{12}^+ \sim 1/(\kappa y^+)$, $L_{vK}^+ \sim \kappa y^+$, as confirmed by the figure 3a. The functions $\ell_{vK}^+(y^+)$ (figure 3a) or $\ell_{vK}(y/\delta)$ (figure 3b), that depend on the flow case and Reynolds-number, have been computed using the accurate expressions of S^+ of the equation (7) of Heinz (2018). In channel or pipe flow, U presents a maximum at the centerplane or pipe axis $y = \delta$, hence S and ℓ_{vK} vanish there. On the contrary, in boundary layer flow, S and ℓ_{vK} vanish only in the limit $y \to \infty$. The figure 3c suggests that, because the dimensional factor in $D_{\nu i}$ (17a), P_ν (first expression in 17b) and $D_{\nu o}$ (first expression in 17c) are respectively ν_t^2/L_{vK}^2 , $\nu_t^2/(L_{vK}\delta)$ and ν_t^2/δ^2, in the ratii δ^2/L_{vK}^2 , δ/L_{vK} , 1, those will peak in the inner, intermediate and outer regions; this will be confirmed in the figures 6 for channel flow, 7 for pipe flow, 8 for boundary layers.
Another ingredient in $D_{\nu i}$ (17a), is the universal damping function

$$f \;=\; f(y^+) \;=\; (1 - S_{12}^+) \left(\frac{(S_{12}^+ - 1)\; S_{12}^+\; d^2 S_{12}^+/dy^{+2}}{(dS_{12}^+/dy^+)^2} + 3 - 2S_{12}^+ \right)^{-1/2} . \tag{19}$$

It is plotted on the figures 4ab. It does tend to zero as $y^+ \to 0$ and 1 as $y^+ \to \infty$.
Finally, in P_ν (17b) and $D_{\nu o}$ (17c) the rightmost functions depend only on W and its derivatives. In P_ν there appears $-4W'$ which is positive according to the figure 2b, hence $P_\nu > 0$ as required. In $D_{\nu o}$ there appears $W'^2 + WW''$ which is plotted on the figure 4c. As already suggested at the level of (16,17), the function $W'^2 + WW'' > 0$ except in a more or less narrow near-wall region, depending on the flow case.

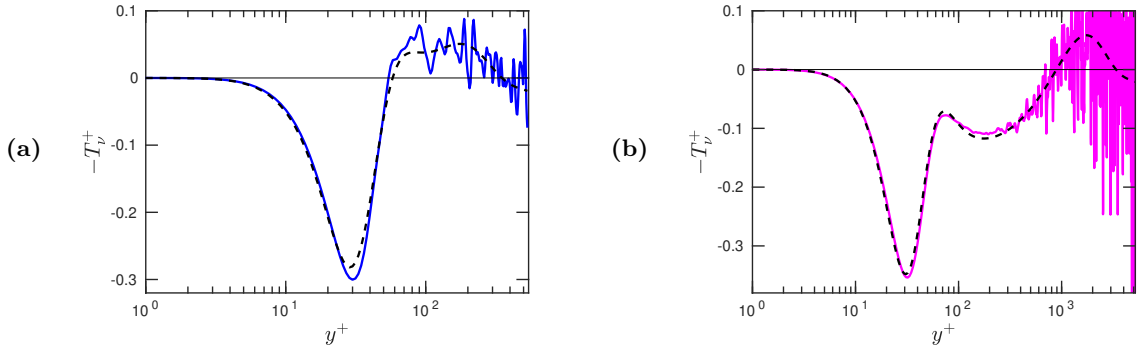

Fig. 5 : The continuous line shows the opposite of the dimensionless turbulent diffusion term $-T_\nu^+$ (20) computed with the channel flow DNS of Lee & Moser (2015) at $Re_\tau = 543$ **(a)**, 5186 **(b)**. The dashed line shows the same term computed with our model (21).

3.2 Application to channel flows

In typical channel flow cases, a comparison of the opposite of the dimensionless turbulent diffusion term

$$-T_\nu^+ \;=\; -\frac{\partial}{\partial y^+}\Big(\nu^+\frac{\partial \nu^+}{\partial y^+}\Big) \tag{20}$$

computed with finite differences from two DNS of Lee & Moser (2015) and its model (16,17),

$$-T_\nu^+ \;=\; P_\nu^+ \;-\; D_\nu^+ \;=\; -\;D_{\nu i}^+ \;+\; P_\nu^+ \;-\; D_{\nu o}^+ \tag{21}$$

is shown on the figures 5. Except in the outer region, where the DNS noise is amplified, there is a good agreement between the model and the DNS, especially, for the highest Reynolds number case.
The separation of $-T_\nu^+$ into the three terms of the model, $-D_{\nu i}^+$, P_ν^+ and $-D_{\nu o}^+$, is illustrated on the figures 6. The comparison of the figures 6a, c and g shows that the dissipation term $D_{\nu i}^+$ dominates in the near-wall region. In this region, and in inner scalings, $D_{\nu i}^+(y^+)$, $D_\nu^+(y^+)$ and $T_\nu^+(y^+)$ approach as $Re_\tau \to \infty$ a limit profile, with a maximum around $y^+ = 31$ and a minimum around $y^+ = 72$. A plateau around $y^+ \simeq 300$ and

$$D_{\nu i}^+ \;\simeq\; D_\nu^+ \;\simeq\; T_\nu^+ \;\simeq\; \kappa^2$$

builds up as $Re_\tau \to \infty$, in agreement with the formula for the log-layer reduced eddy viscosity, $\nu^+ = \kappa y^+$. For larger values of y/δ, after this plateau, the figures 6bdfh show that all terms, considered in inner-outer scalings, $D_{\nu i}^+(y/\delta)$, $D_{\nu o}^+(y/\delta)$, $D_\nu^+(y/\delta)$, $P_\nu^+(y/\delta)$ and $T_\nu^+(y/\delta)$, approach limit profiles as $Re_\tau \to \infty$.

3.3 Application to pipe flows

In the eddy-viscosity model (9), the only difference between channel and pipe flows is described by the change of the coefficient K_X in the function W_X (13) that contains the wake effects. This change from $K_C = 0.933$ to $K_P = 0.687$ is moderate, therefore the turbulent diffusion term and its contributions are close to the ones of channel flow, as shows the comparison between the figures 6 and figures 7. All the comments made on the figures 6 at the end of section 3.2 also apply to the figures 7.

3.4 Application to boundary layers

The boundary layer case differs from the channel and pipe flow cases in that the maximum value of y (resp. y^+) is not δ (resp. $\delta^+ = Re_\tau$) but, in principle, infinity. Moreover, the wake function W of boundary layers (14) differs significantly from the one of channel and pipe flows (13). The comparison of the figures 8 with the figures 6 and 7 shows similar behaviours in the ranges $y \in [0, \delta[$ i.e. $y^+ \in [0, \delta^+[$, whereas there are differences in the outer region. At $y = \delta$, i.e. the centerplane in channels or the pipe axis in pipes, the function T_ν should present a vanishing slope for symmetry reasons, as confirmed by the figures 6h and 7h; note that the outer term $-D_{\nu o}^+$ plays an important role there. In boundary layers, one does not expect a similar property, but that T_ν should approach 0 as $y \to \infty$. This is what suggests the figure 8h, and what would confirm a figure drawn with a larger interval of the abscissas (not shown): for all the Reynolds numbers implied, that range from 543 to 30000, $|T_\nu^+| < 10^{-3}$ as soon as $y > 1.32\delta$.

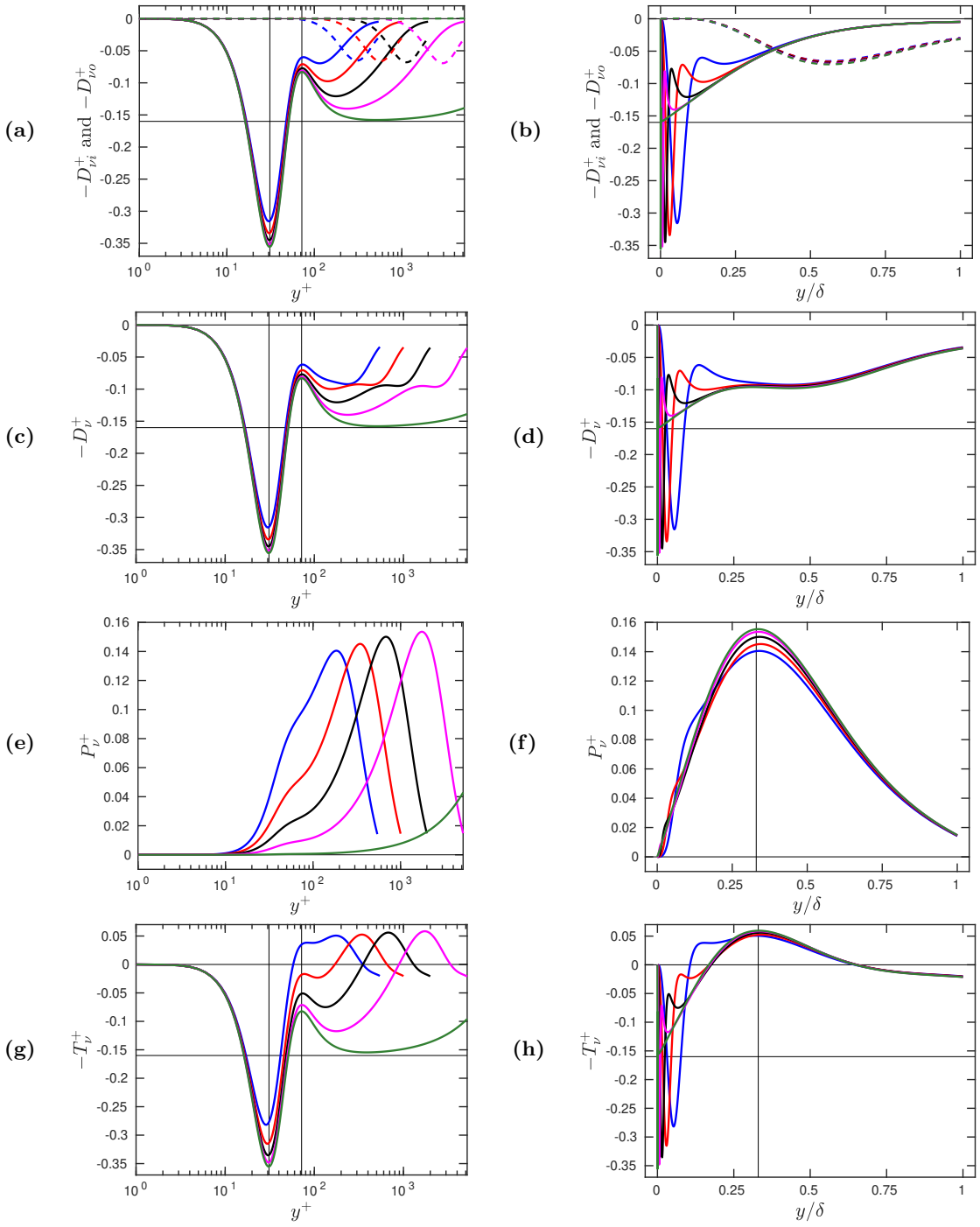

Fig. 6 : For channel flows at $Re_\tau = 543$ (blue), 1001 (red), 1995 (black), 5186 (magenta), 80000 (green), the various contributions to $-T_\nu^+$ (21) and their sum. **(a,b)** $-D_{\nu i}^+$ with the continuous, $-D_{\nu o}^+$ with the dashed lines. **(c,d)** $-D_\nu^+$. **(e,f)** P_ν^+ . **(g,h)** $-T_\nu^+$. On **(a,c,g)** the vertical lines are at $y^+ = 31$ and 72; on **(f,h)** they are at $y = 0.33\delta$. On **(a,b,c,d,g,h)** the horizontal lines are at $-T_\nu^+ = 0$ and $-\kappa^2$.

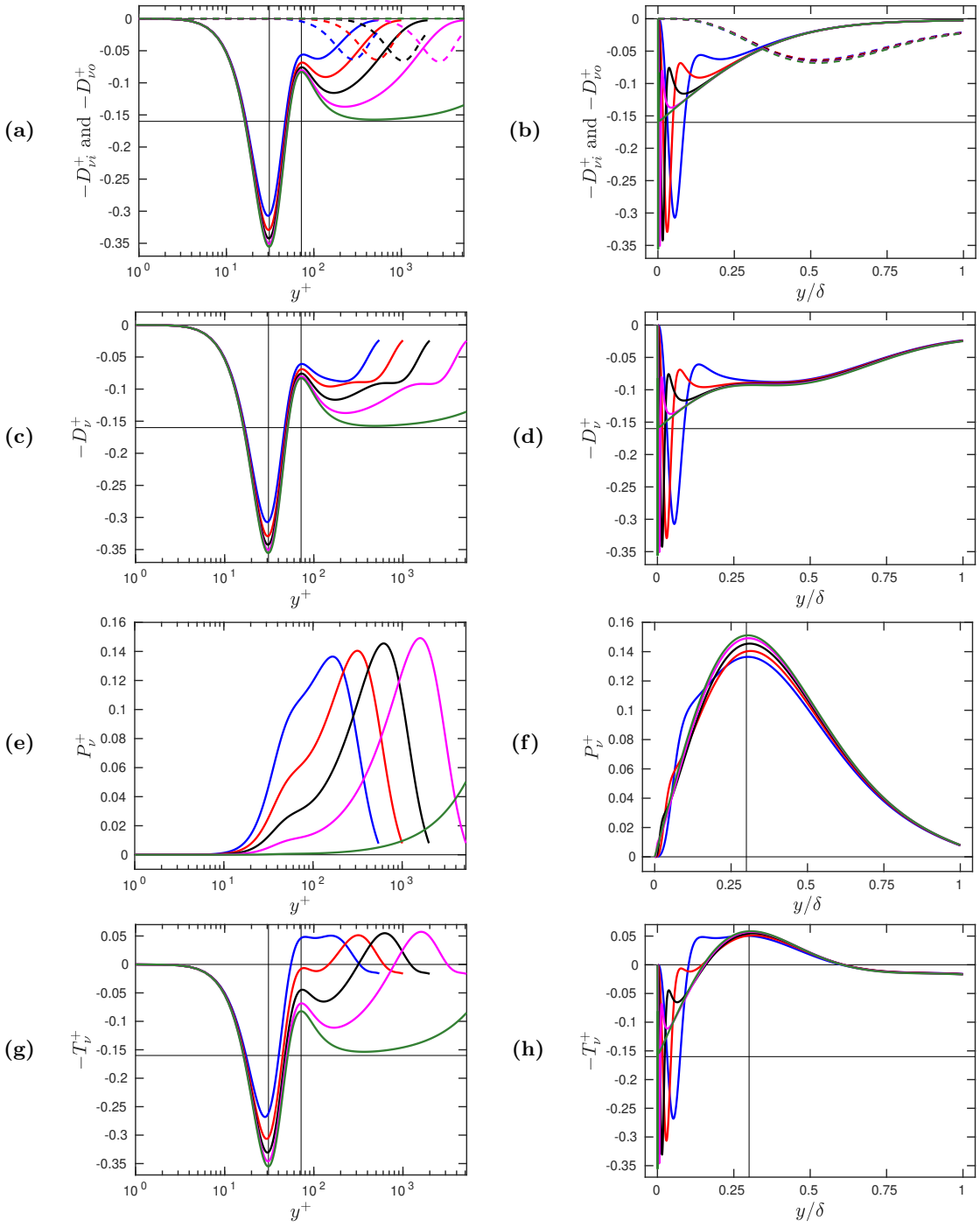

Fig. 7 : Same as figure 6, but for pipe flows. On **(f,h)** the vertical lines are at $y = 0.3\delta$.

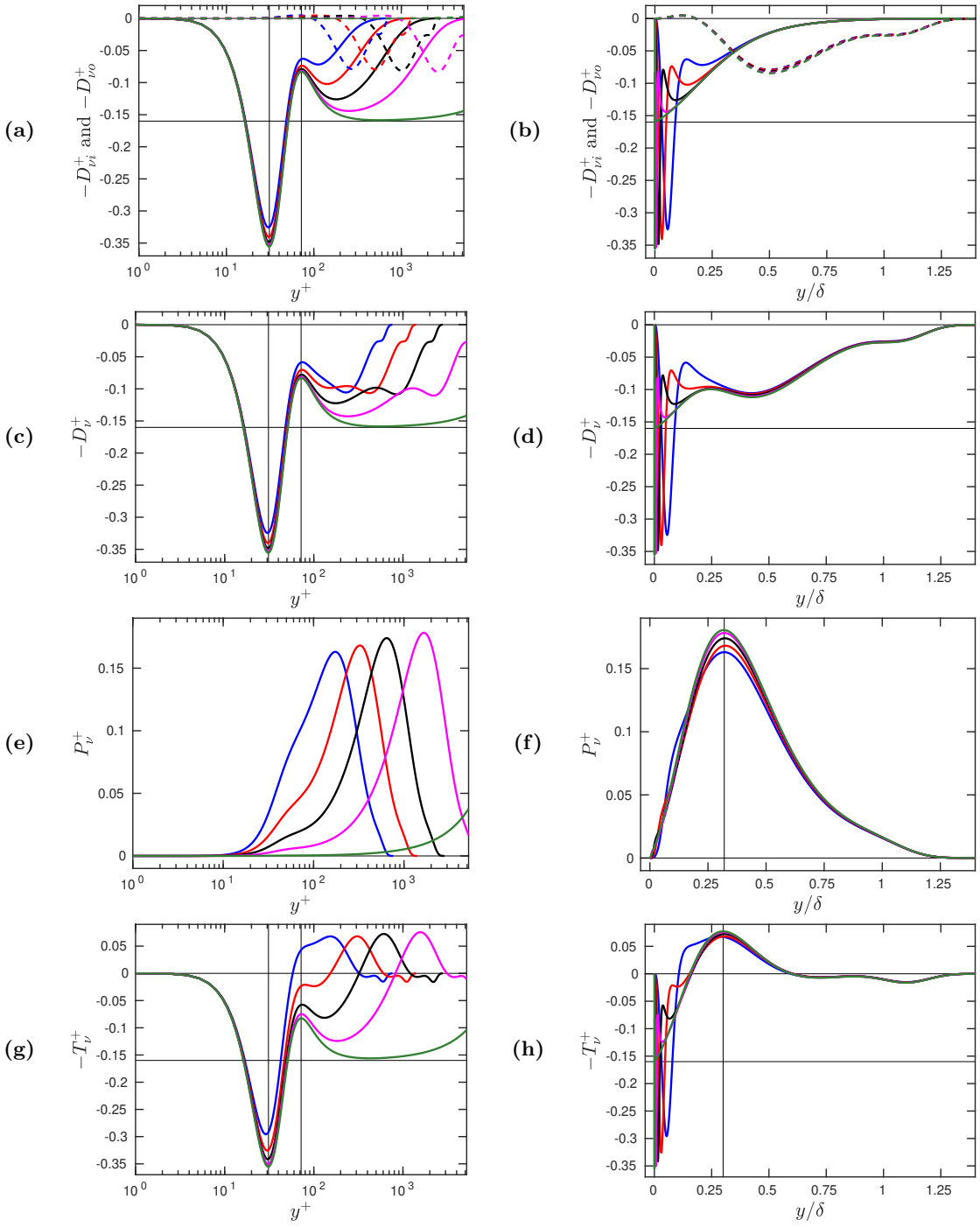

Fig. 8 : Same as figure 6, but for boundary layers; in all graphs $1 \leq y^+ \leq 1.4\delta^+$. On **(f)** the vertical line is at $y = 0.32\delta$, on **(h)** it is at $y = 0.3\delta$.

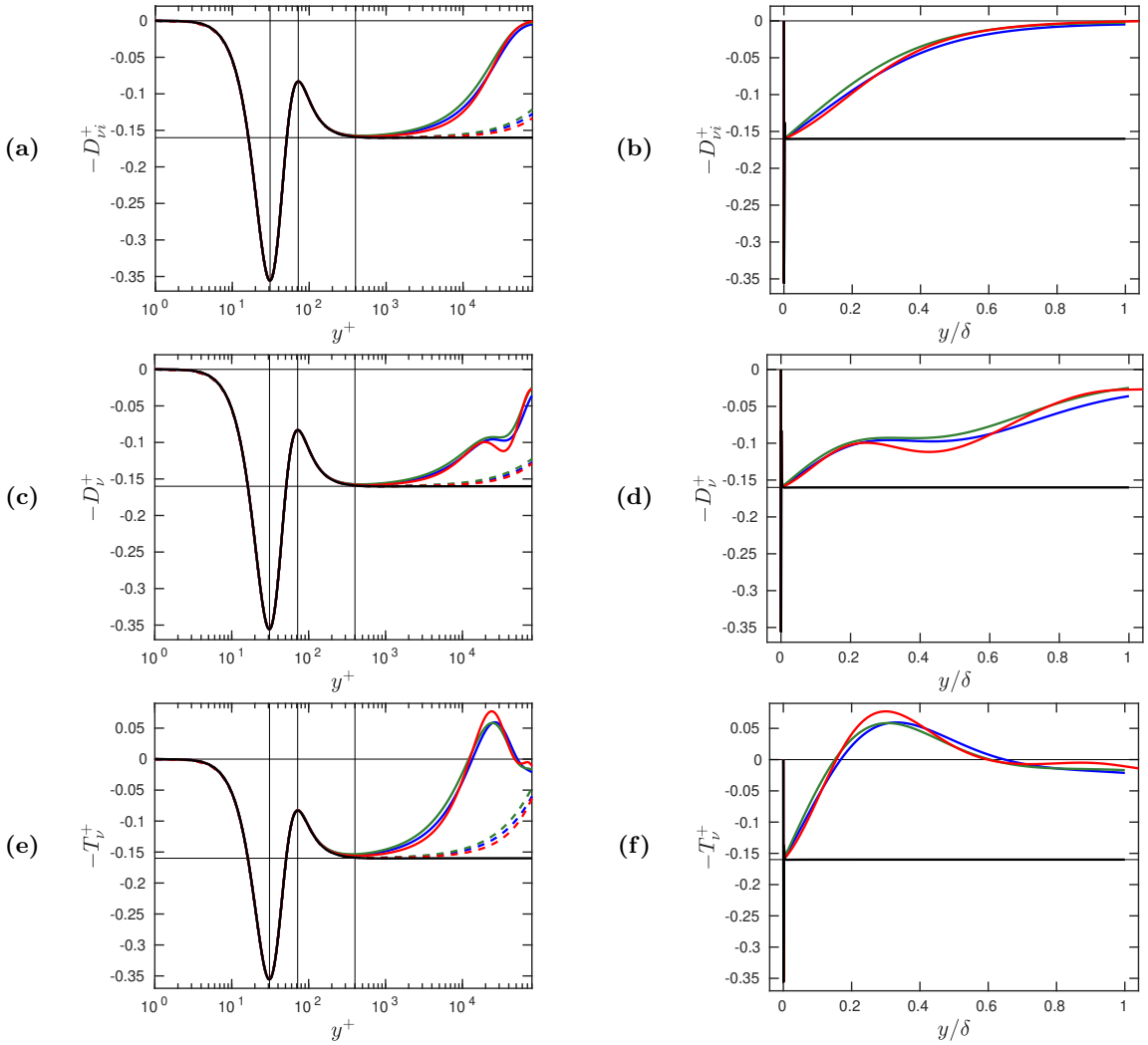

Fig. 9 : The black curves show $-D^+_{\nu ia}$, see (22), calculated with $Re_\tau = 80000$ in **(b,d,f)**. The blue curves for channel flow, green curves for pipe flow, red curves for boundary layer show, with $Re_\tau = 80000$, in **(a,b)** $-D^+_{\nu i}$, **(c,d)** $-D^+_{\nu}$, **(e,f)** $-T^+_{\nu}$. On **(a,c,e)** the curves of $-D^+_{\nu i}$, $-D^+_{\nu}$ and $-T^+_{\nu}$ for $Re_\tau = 800000$ have been added with dashed lines, and the same color codes; the vertical lines are at $y^+ = 31,\ 72$ and 400, the horizontal lines are at $-T^+_{\nu} = 0$ and $-\kappa^2$.

3.5 Asymptotic structure of the near-wall dissipation

The figures 6acg, 7acg and 8acg show that, as $Re_\tau \to \infty$, the dissipation dominates the eddy-viscosity budget in the near-wall region, the near-wall dissipation scales with y^+, and it approaches a universal asymptotic profile. This profile is obtained by replacing, in the expression (9) of the eddy-viscosity, which appears at the power 2 in $D_{\nu i}$ (17a), the wake function W by 1, since then the wake region goes to infinity in inner scaling. This yields, as a relevant approximation of $D_{\nu i}$, the asymptotic dissipation function

$$D_{\nu ia} \;=\; \kappa^2\,\frac{\nu^2}{L_{vK}^2}\,\frac{(1/S_{12}^+ - 1)^2}{f^2} \qquad \text{or} \qquad D^+_{\nu ia} \;=\; \kappa^2\,\frac{(1/S_{12}^+ - 1)^2}{L_{vK}^{+2}}\,\frac{1}{f^2}\ . \tag{22}$$

It is universal in that it does not depend on the flow case, but only on S_{12}^+ , see the equations (10), (18) and (19). Moreover $D^+_{\nu ia}$ considered as a function of y^+ also does not depend on Re_τ . As $y^+ \to \infty$, since $1/S_{12}^+ - 1$ and L_{vK}^+ approach κy^+, whereas $f \to 1$, one has $D^+_{\nu ia} \to \kappa^2$, in agreement with the expression of the log-layer eddy viscosity. This is visible on the figures 9ace; more precisely, $|D^+_{\nu ia} - \kappa^2| < 10^{-3}$ as soon as $y^+ \geq 400$. The colored curves in figures 9ace confirm that, at fixed y^+, $D_{\nu i}$, D_ν and T_ν approach, as $Re_\tau \to \infty$, $D_{\nu ia}$, whatever the flow case. We have not plotted the curves for $Re_\tau = 800000$ on figures 9bdf, since they are indistinguishable, in outer scaling, from the curves for $Re_\tau = 80000$. From a physical point of view, these results suggest that near-wall dissipation is due to universal near-wall motions.

The differences between T_ν and $-D_{\nu ia}$ in the outer region, visible on the figure 9f, are due to the contribution of the production P_ν and outer dissipation $-D_{\nu o}$, which are now studied in the limit $Re_\tau \to \infty$.

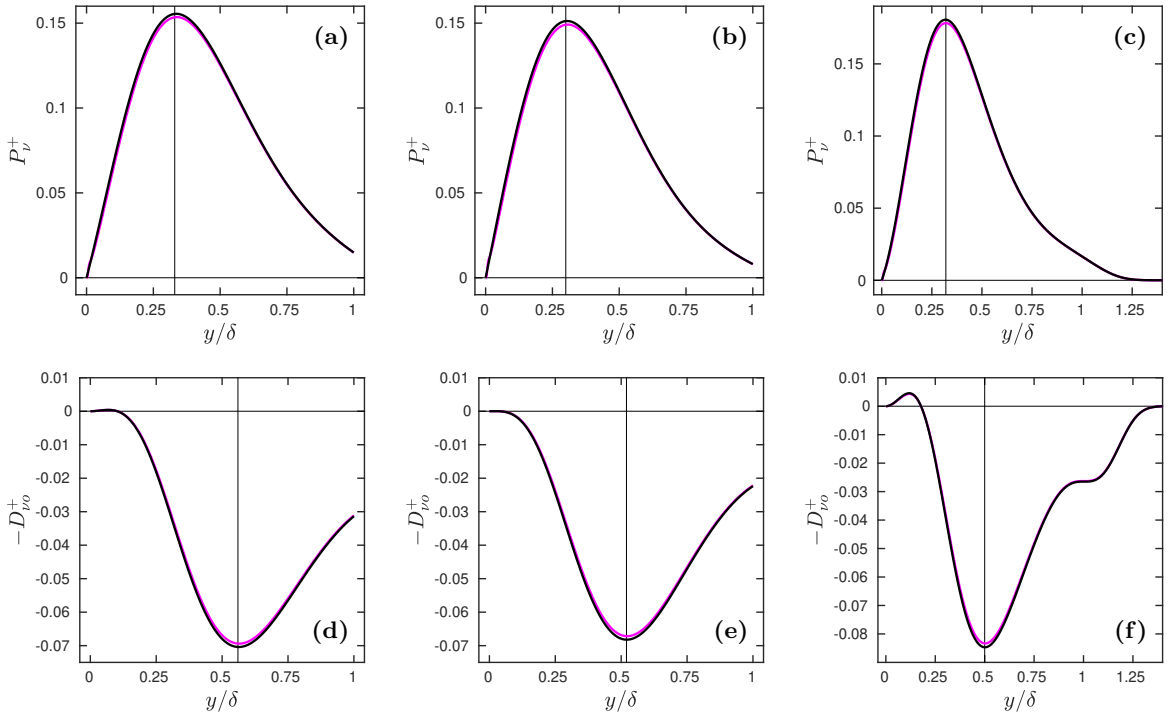

Fig. 10 : For channel flow **(a,d)**, pipe flow **(b,e)**, boundary layer **(c,f)**. The black curves show $P_{\nu a}^+$, see (24), the magenta curves P_ν^+ for $Re_\tau = 5186$ in **(a,b,c)**. The black curves show $-D_{\nu oa}^+$, see (26), the magenta curves $-D_{\nu o}^+$ for $Re_\tau = 5186$ in **(d,e,f)**. The vertical lines are at $y/\delta = 0.33$ **(a)**, 0.3 **(b)**, 0.32 **(c)**, 0.56 **(d)**, 0.52 **(e)**, 0.5 **(f)**.

3.6 Asymptotic structure of the production

The figures 6ef, 7ef and 8ef show that, as $Re_\tau \to \infty$, the production of the eddy viscosity vanishes in the near-wall region, scales with y/δ, and approaches asymptotic profiles that depend only on the flow case. These profiles are obtained by replacing, in the second expression of P_ν (17b), transformed in inner units,

$$P_\nu^+ \;=\; \kappa \, \frac{\nu^+}{S_{12}^+ \; L_{vK}^+ \; \delta^+} \; (-4W') \; , \tag{23}$$

the eddy viscosity ν^+, the strain rate S_{12}^+ and the von Karman length-scale L_{vK}^+ by their approximations valid as $y^+ \to \infty$, i.e. $\kappa y^+ \; W$, $1/\kappa y^+$ and κy^+ respectively, see the discussions after equations (9-12) for ν^+ and S_{12}^+ , equation (18) for L_{vK}^+ . This yields the asymptotic profiles

$$P_{\nu a}^+ \;=\; \kappa^2 \, \frac{y}{\delta} \; (-4WW') \quad \text{or} \quad P_{\nu a} \;=\; \kappa^2 \; u_\tau^2 \, \frac{y}{\delta} \; (-4WW') \; . \tag{24}$$

The first equation shows that $P_{\nu a}^+$ is, for a fixed flow case, a function of y/δ only, because the wake function W depends only on y/δ, see equations (13) and (14). The figures 10abc confirm that, at fixed y/δ, P_ν^+ approaches $P_{\nu a}^+$ as $Re_\tau \to \infty$. For $Re_\tau = 80000$, the profiles of P_ν^+ for the three flow cases are indistinguishable from the corresponding functions $P_{\nu a}^+$ at the scale of the figures 10abc. From a physical point of view, these results suggest that production is due to large-scale outer motions. The comparison between the vertical scales of the figures 10abc also suggest that these motions contribute more efficiently to the production of ν_t in the boundary layer than in the other flows. This is probably related to the fact that the boundary layer is in principle unbounded in the wall-normal direction, contrarily to channel and pipe flows.

3.7 Asymptotic structure of the outer dissipation

The figures 6ab, 7ab and 8ab show that, as $Re_\tau \to \infty$, the outer dissipation of the eddy viscosity vanishes in the near-wall region, scales with y/δ, and approaches asymptotic profiles that depend only on the flow case. These profiles are obtained by starting from the second expression of $D_{\nu o}$ (17c), transformed in inner units,

$$D_{\nu o}^+ \;=\; \frac{1}{\delta^{+2}} \; (1/S_{12}^+ - 1)^2 \; (W'^2 + WW'') \; , \tag{25}$$

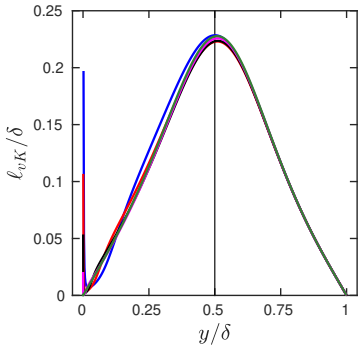

Fig. 11 : For channel flows at $Re_\tau = 543$ (blue), 1001 (red), 1995 (black), 5186 (magenta), 80000 (green), the von Karman length scale ℓ_{vK} (6). All plots start at $y^+ = 1$.

and applying one of the approximations that led from (23) to (24), i.e. replacing $1/S_{12}^+ - 1$ by κy^+. This yields the asymptotic profiles

$$D^+_{\nu oa} \;=\; \kappa^2 \left(\frac{y}{\delta}\right)^2 (W'^2 + WW'') \quad \text{or} \quad D_{\nu oa} \;=\; \kappa^2\, u_\tau^2 \left(\frac{y}{\delta}\right)^2 (W'^2 + WW'') \;. \tag{26}$$

Similar to $P^+_{\nu a}$ (24), $D^+_{\nu oa}$ is, for a fixed flow case, a function of y/δ only. The figures 10def confirm that, at fixed y/δ, $D^+_{\nu o}$ approaches $D^+_{\nu oa}$ as $Re_\tau \to \infty$. For $Re_\tau = 80000$, the profiles of $D^+_{\nu o}$ for the three flow cases are indistinguishable from the corresponding functions $P^+_{\nu a}$ at the scale of the figures 10def. From a physical point of view, this contribution to the dissipation is probably due to large-scale outer motions.

4 Models of the production term

From now on the text is less finalized / this section is ***exploratory*** *!*

From now on, the focus is on channel flows, for which the high-quality DNS of Lee & Moser (2015) are available. Our aims in this section are a review of existing models of the production term, to show that they lack some length-scale information, and to propose length-scale factors to try to construct a general model of the production term in the eddy-viscosity equation for wall-bounded turbulent flows. Inspired by the fact that the asymptotic von Karman length scale L_{vK} plays an important role in the exact model, it seems natural to imply the von Karman length scale ℓ_{vK} in a more general model. These length scales have been plotted in the figures 3ab for various flow cases. The figure 11 completes the figure 3b and shows that ℓ_{vK} always presents (disregarding a narrow near-wall region) a simple profile, robust versus Reynolds number changes, that peaks around $y \simeq 0.5\delta$.

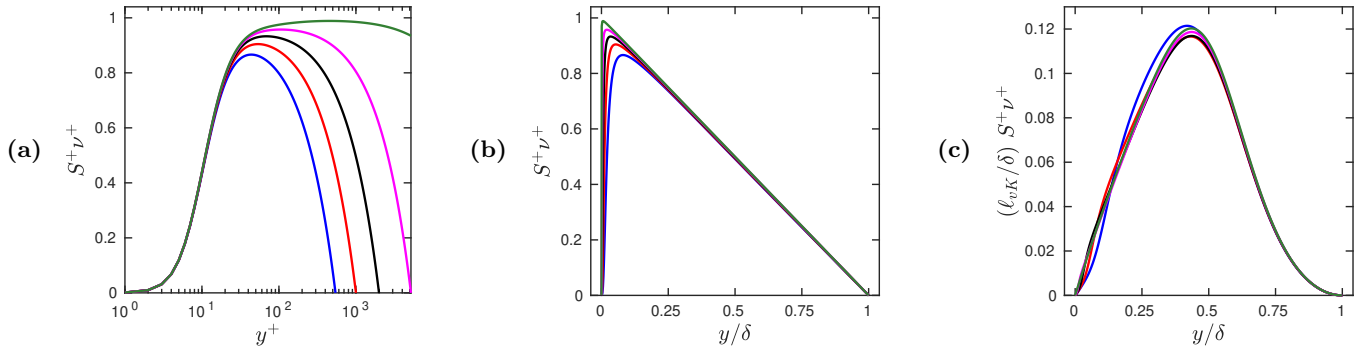

Fig. 12 : For the channel flows cases of figure 11, with the same color codes, the base function $S^+\ \nu^+$ in the production term $P^+_{\nu SA}$ of Spalart & Allmaras (1994), see equation (27), in **(a,b)**; the same after multiplication by the length-scale factor ℓ_{vK}/δ in **(c)**. All plots start at $y^+ = 1$.

4.1 About the model of Spalart & Allmaras (1994)

The high-Reynolds number eddy-viscosity equation (4) of Spalart & Allmaras (1994) contains the production term

$$P_{\nu SA} \ = \ C_{b1}\ S\ \nu_t \tag{27}$$

where $C_{b1} \ = \ \sigma\ c_{b1}$ with their notations. The base function $S\ \nu_t$ is one of the simplest possible choices for a model of $\partial\nu_t/\partial t$, see equation (15). The figures 12ab show this function vs y^+ and y/δ; it has been computed using for S^+ the accurate expression of the equation (7) of Heinz (2018). The comparison of the figures 12ab with the figures 6ef suggests that there misses a length-scale factor in (27), that could lead to a peak not confined to the near-wall region but at a finite value of y/δ. A reasonable length-scale factor could be the scaled von Karman length-scale ℓ_{vK}/δ, which has been plotted in the figure 11. Indeed it is small in the near-wall region and peaks around $y \simeq 0.5\delta$. The product $(\ell_{vK}/\delta)\ S^+\ \nu^+$ plotted in the figure 12c does show strong similarities with the exact production term displayed in the figure 6f. Such a model for P_ν ,

$$P_{\nu SAmodified} \ = \ C_{b1}\ (\ell_{vK}/\delta)\ S\ \nu_t\ , \tag{28}$$

is not entirely satisfactory, however, since the factor δ is nonlocal.

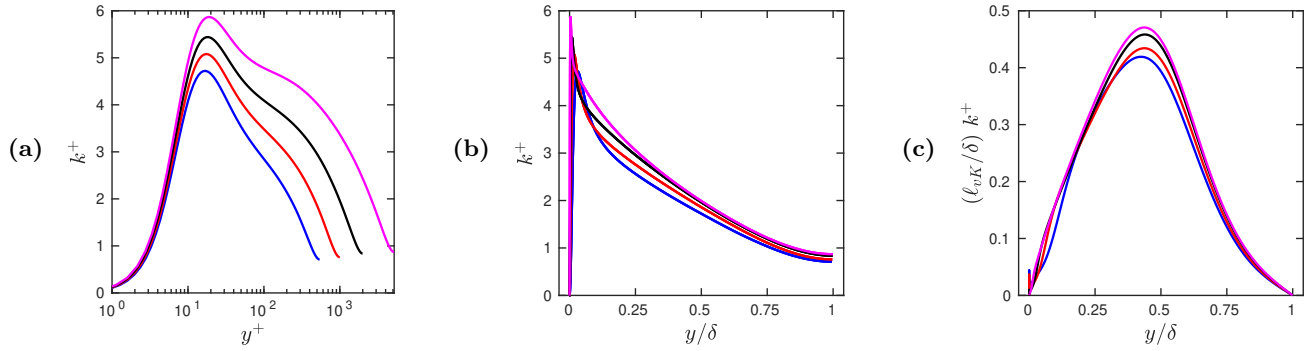

Fig. 13 : For the channel flow DNS of Lee & Moser (2015) at $Re_\tau = 543$ (blue), 1001 (red), 1995 (black), 5186 (magenta), the turbulent kinetic energy k^+ in the production term $P^+_{\nu Y}$ of Yoshizawa *et al.* (2012), see equation (29), in **(a,b)**; the same after multiplication by the length-scale factor ℓ_{vK}/δ in **(c)**. All plots start at $y^+ \simeq 1$.

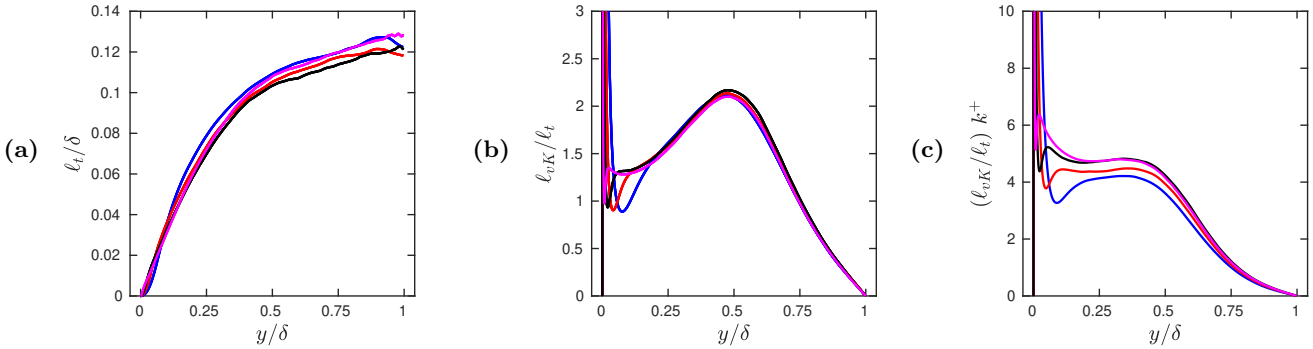

Fig. 14 : For the channel flow DNS of Lee & Moser (2015) already studied in the figures 13, the ratio of the turbulent length-scale ℓ_t (5) with δ in **(a)**, the ratio ℓ_{vK}/ℓ_t in **(b)**, the product $(\ell_{vK}/\ell_t)\ k^+$ in **(c)**.

4.2 About the model of Yoshizawa *et al.* (2012)

The model of Yoshizawa *et al.* (2012) implies three turbulent fields: the eddy viscosity ν_t (as Spalart & Allmaras 1994), the turbulent kinetic energy k and the turbulent dissipation ϵ. It also proposes an eddy-viscosity equation, their equation (19), which was shown to yield a better model of ν_t than the eddy-viscosity formula of the standard $k-\epsilon$ model in some specific cases. In this eddy-viscosity equation, the production term is

$$P_{\nu Y} \ = \ c_{\nu P}\ k \tag{29}$$

where $c_{\nu P} \ = \ \sigma\ C_{\nu P}$ with their notations. Indeed, the turbulent kinetic energy k is from a dimensional and physical point of view another reasonable choice for a model of $\partial\nu_t/\partial t$. The profiles of k^+ shown in the figures 13ab are similar to those of $S^+\ \nu^+$ shown in the figures 12ab, in that they peak in the near-wall region. The comparison of the figures 13ab with the figures 6ef suggests that there misses a length-scale factor in (27), that could lead to a peak at a finite value of y/δ. Using ℓ_{vK}/δ as the length-scale factor, as we did it already for the model of Spalart & Allmaras (1994), leads to the figure 13c, which is again similar to the figure 6f displaying the exact production term.

In order to obtain a local model, one might replace ℓ_{vK}/δ by the ratio of the von Karman length-scale ℓ_{vK} with the turbulent length-scale ℓ_t (5), which may be computed from ν_t and k that are available in the model of Yoshizawa *et al.* (2012). The profiles of ℓ_t (5), computed with the DNS data of Lee & Moser (2015), are shown on the figure 14a. One may then compute the length-scale ratio ℓ_{vK}/ℓ_t shown in the figure 14b. It behaves like ℓ_{vK}/δ in the outer region, compare with the figure 3b, but is much larger in the near-wall region. Consequently $(\ell_{vK}/\ell_t)\ k^+$, displayed in the figure 14c, has not the desired behaviour.

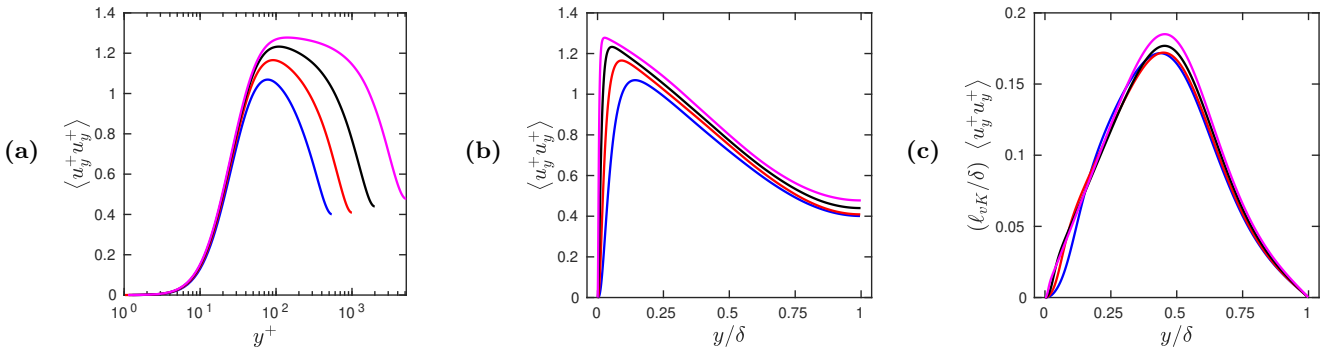

Fig. 15 : For the channel flow DNS of Lee & Moser (2015) already studied in the figures 13, the variance $\langle u_y^+ u_y^+ \rangle$ in the production term $P_{\nu H}^+$ of Hamba (2013), see equation (30), in **(a,b)**; the same after multiplication by the length-scale factor ℓ_{vK}/δ in **(c)**.

4.3 About the model of Hamba (2013)

Hamba (2013) proposed an eddy-viscosity equation (his equation 37) with the production term

$$P_{\nu H} \;=\; \sigma\ \langle u_y u_y \rangle\,. \tag{30}$$

The base function $\langle u_y u_y \rangle$ is (up to a factor 2) a contribution to the turbulent kinetic energy k, hence this production term is similar in principle to the one of Yoshizawa *et al.* (2012) equation (29). Similarly to k^+, $\langle u_y^+ u_y^+ \rangle$ peaks in the near-wall region: compare the figures 13ab and figures 15ab. The comparison with the figures 6ef suggests that there misses a length-scale factor in (27), that could lead to a peak at a finite value of y/δ. Using ℓ_{vK}/δ as the length-scale factor, as we did it already for the models of Spalart & Allmaras (1994) and Yoshizawa *et al.* (2012), leads to the figure 15c, which is again similar to the figure 6f displaying the exact production term.

References

Abdol-Hamid, K. S. 2015 Assessments of $k-kL$ Turbulence Model Based on Menter's Modification to Rotta's Two-Equation Model. *Int. J. Aerospace Engineering* **2015**, 1–18, http://downloads.hindawi.com/journals/ijae/2015/987682.pdf.

Baldwin, B. & Barth, T. 1990 A one-equation turbulence transport model for high Reynolds number wall-bounded flows. *NASA Technical Memorandum* pp. 102847, 1–20.

Chin, C., Monty, J. & Ooi, A. 2014 Reynolds number effects in DNS of pipe flow and comparison with channels and boundary layers. *Int. J. Heat & Fluid Flow* **45**, 33 – 40.

Egorov, Y., Menter, F., Lechner, R. & Cokljat, D. 2010 The scale-adaptive simulation method for unsteady turbulent flow predictions. Part 2: Application to complex flows. *Flow, Turbulence & Comb.* **85**, 139–165.

Hamba, F. 2013 Exact transport equation for local eddy viscosity in turbulent shear flow. *Phys. Fluids* **25**, 085102.

Heinz, S. 2018 On mean flow universality of turbulent wall flows. I. High Reynolds number flow analysis. *J. Turbulence* **19**, 929–958.

Heinz, S. 2019 On mean flow universality of turbulent wall flows. II. Asymptotic flow analysis. *J. Turbulence* **20**, 174–193.

Lee, M. & Moser, R. D. 2015 Direct numerical simulation of turbulent channel flow up to $Re_\tau \approx 5200$. *J. Fluid Mech.* **774**, 395–415.

Menter, F. & Egorov, Y. 2006 Revisiting the turbulent scale equation. *IUTAM Symposium on One Hundred Years of Boundary Layer Research*, pp. 279–290. Springer.

Menter, F. R. 1997 Eddy viscosity transport equations and their relation to the $k-\epsilon$ model. *J. Fluids Eng.* **119**, 876–884.

Menter, F. R. & Egorov, Y. 2010 The scale-adaptive simulation method for unsteady turbulent flow predictions. Part 1: theory and model description. *Flow, Turbulence & Comb.* **85**, 113–138.

Nee, V. W. & Kovasznay, L. S. G. 1969 Simple phenomenological theory of turbulent shear flows. *Phys. Fluids* **12**, 473–484.

Sillero, J. A., Jiménez, J. & Moser, R. D. 2013 One-point statistics for turbulent wall-bounded flows at Reynolds numbers up to $\delta^+ \simeq 2000$. *Phys. Fluids* **25**, 105102,1–16.

Spalart, P. & Allmaras, S. 1994 A one-equation turbulence model for aerodynamic flows. *Recherche Aérospatiale* **1**, 5–21.

Vallikivi, M., Hultmark, M. & Smits, A. J. 2015 Turbulent boundary layer statistics at very high Reynolds number. *J. Fluid Mech.* **779**, 371–389.

Yoshizawa, A., Abe, H., Matsuo, Y., Fujiwara, H. & Mizobuchi, Y. 2012 A Reynolds-averaged turbulence modeling approach using three transport equations for the turbulent viscosity, kinetic energy, and dissipation rate. *Phys. Fluids* **24**, 075109.

Archives: links to important previous versions

- **V0.085 of June 4, 2020:** memory of the **section 3.8 QR6 on the BL case inspired from Spalart & Allmaras (1994)** - possible advection effects that might change the lhs of the ν_t eq.
- **V0.055 of May 19, 2020:** memory of the **section 4.1 Comparison with Hamba (2013)**, of **figure 9** for P_ν and $P_{\nu H}$, of **QR5** regarding this comparison.
- **V0.025 of May 7, 2020:** memory of **figure 5** for W'/W and $(W'^2+WW'')/W^2$, **QR3** regarding comparisons with DNS of pipe flow, **QR4** regarding comparisons with DNS of BL, **figure 10** for $-T_\nu^+$ et al. in BL with an extended range of y^+.
- **V0.015 of April 29, 2020:** memory of **QR1** regarding near-wall effects / the kinematic viscosity & **QR2** regarding pipe flow / curvature effects.